PCCP

Accepted Manuscript

ROYAL SOCIETY OF CHEMISTRY

www.rsc.org/pccp

Journal Name

RSCPublishing

ARTICLE

Negligible degradation on *in situ* voltage cycling of a PEMFC with electrospun niobium-doped tin oxide supported Pt cathode

Cite this: DOI: 10.1039/x0xx00000x

Received 00th January 2012,
Accepted 00th January 2012

DOI: 10.1039/x0xx00000x

www.rsc.org/

Iuliia Savych, [a] Surya Subianto, [a] Yannick Nabil, [a] Sara Cavaliere, [a,*] Deborah Jones, [a] Jacques Rozière[a]

Novel platinum-catalysed corrosion-resistant loose-tube-structured electrocatalysts for proton exchange membrane fuel cells have been obtained using single-needle electrospinning associated with a microwave-assisted polyol method. Monodisperse platinum particles supported on Nb-SnO_2 demonstrated higher electrochemical stability than conventional Pt/C electrodes during *ex situ* potential cycling and comparable activity in the oxygen reduction reaction. *In situ* fuel cell operation under accelerated stress test conditions of a membrane electrode assembly elaborated with a Pt/C anode and Pt/Nb-SnO_2 cathode confirmed that voltage loss is significantly lower with the novel cathode than with an MEA prepared with conventional Pt/C supported electrocatalysts. Furthermore, the Nb-SnO_2 stabilized the supported platinum nanoparticles against dissolution, migration and reprecipitation in the membrane. Pt/Nb-SnO_2 loose-tubes constitute a mitigation strategy to two known degradation mechanisms in PEMFC: corrosion of the carbon support at the cathode, and dissolution of Pt at high cell voltages.

Introduction

Fuel cell electrocatalyst support materials are required to have high electronic conductivity, specific surface area, electrochemical and chemical stability under operating conditions and the ability to form a layer with the required porous structure to allow reactant gas ingress and product water egress. Carbon blacks have been successful at providing these properties, with the notable exception of electrochemical stability at high potentials. High potentials can arise at both anode and cathode during fuel cell operation, for example under stop/start conditions.

Whilst some mitigation strategies within the MEA are possible, such as using catalyst that doesn't promote ORR on the anode, carbon corrosion is not prevented in this way, only reduced. Transition metal oxides[1] are more stable under cell reversal and start/stop conditions which explains the current high interest in the development of synthesis approaches leading to transition metal oxides of high surface area and relatively high electronic conductivity such as TiO_2[2–4], WO_2[5–7], SnO_2[8–11]. A recent study on the platinum aggregation and redispersion on a range of metal oxide surfaces under the operating conditions of PEMFC cathodes showed that NbO_2 and SnO_2 are good redispersion supports[12]. They could, furthermore, play a co-catalyst role and promote the electrocatalytic reaction as a result of a strong metal-support interaction (SMSI)[13]. Doping tin oxide with aliovalent ions (Sb, Nb, Ta and Ru etc.) is an effective approach[14–18] to increasing its electronic conductivity to that required for efficient electron transfer at the electrode. Several recent *ex situ* studies into the use of doped tin oxide as electrocatalyst support for cathode of proton exchange membrane fuel cells have concluded that Pt supported on Nb/SnO_2, Sb/SnO_2 and Ru/SnO_2 demonstrates good activity for oxygen reduction reaction

(ORR)[8,9,16,17,19,20] and greater stability on cycling to high cell voltage than Pt/C electrocatalysts.

One-dimensional structures such as nanofibres and nanotubes have demonstrated unique electrical properties and high specific surface area[21]. Pt supported on SnO_2 nanowires directly grown on carbon-paper fuel cell backings exhibited higher activity for ORR than a standard Pt/C electrode[11]. An efficient technique to prepare 1D nanomaterials with controlled diameters and structures is electrospinning and interest in electrospun ceramic fibres for energy conversion devices has grown dramatically in recent years[22]. While several studies have described the preparation of electrospun TiO_2 fibres for application in PEMFC cathodes[2,23–27], investigation of Pt loaded SnO_2 fibres prepared by electrospinning revealed unique electrocatalytic activity for the hydrogen oxidation reaction while inhibiting the ORR, and are potentially used in the anode side[28, 29].

In recent work we described the elaboration and formation mechanism of an unusual fibre-in-tube ("loose-tube") architectured Nb doped tin oxide obtained by electrospinning[30]. The doping drove the morphology to hollow fibres and also increased the electrical conductivity to 2 10^{-2} S cm^{-1} at RT, a value that is in the range of other recently reported doped SnO_2 nanomaterials[16,18,31]. Preliminary results have shown high electrochemical stability upon voltage cycling of the catalysed supports. In this work, we investigated the ORR activity and the stability over time of Pt electrocatalysts supported on Nb doped SnO_2 loose-tubes in both *ex situ* and *in situ* fuel cell measurements. We reveal from combined electrochemical and electron microscopic characterisation that migration of platinum from the cathode and reprecipitation in the membrane during fuel cell operation under accelerated ageing conditions is significantly lower with the Pt/Nb-SnO_2 support at the cathode than with Pt/C, and conclude that such alternative supports represent a mitigation strategy not only for support corrosion, but also for deleterious loss of catalyst from the cathode to the membrane.

Experimental

Synthesis of Pt/Nb doped SnO_2 loose-tubes

The detailed synthesis of Pt/Nb-doped SnO_2 loose-tubes was reported elsewhere[30]. For the preparation of Nb-SnO_2, 0.78 g of tin(II) chloride (98 %, Sigma-Aldrich) and 0.06 g of niobium(V) chloride (98 % min., Merck) were dissolved in 5.7 mL of absolute ethanol (puriss., Sigma-Aldrich) and added to a solution of 0.8 g of polyvinylpyrrolidone (average M_w ~ 1,300,000, Aldrich) in 3.1 mL of N,N-dimethylformamide (98 % min., Fluka). The resulting mixture was stirred at least for 1 h in order to obtain homogeneous solution. This solution was electrospun at room temperature using an applied voltage of 15 kV, a needle-collector distance of 10 cm and a flow rate of 0.4 mL h^{-1}. The as-spun fibres were calcined at 600 °C for 4 h in air with a heating rate of 5 °C min^{-1}.

A microwave-assisted polyol method was used to synthesize Pt nanocatalyst particles. 130 mg of hexachloroplatinic acid (H_2PtCl_6 $6H_2O$, 99.9 % Alfa Aesar) were dissolved in 90 mL of ethylene glycol (99.5 %, Fluka) and the pH was adjusted to pH 11.4 using 1 M NaOH solution (98 %, Sigma Aldrich) in ethylene glycol. The resulting solution was heated at 120 °C for 6 minutes in a microwave reactor (MiniFlow 200SS Sairem). A suspension containing 112 mg of the Nb-SnO_2 fibres in 5 mL ethylene glycol was added to the as-synthesized Pt nanoparticle suspension and the pH was adjusted to 2. After gentle stirring for 24 hours the product was recovered by filtration, washed with milli-Q water and ethanol and dried at 160 °C for 1 h.

Physico-chemical characterisation of Pt/Nb-SnO_2 loose-tubes

The nanofibre morphology was analysed by FE-SEM using a Hitachi S-4800 scanning electron microscope. Powder X-ray diffraction (XRD) patterns were recorded at room temperature in Bragg-Brentano configuration using a PANAlytical X'pert diffractometer, equipped with a hybrid monochromator, operating with CuK_α radiation (λ = 1.541 Å), and using a step size of 0.1° 2θ within the 2θ domain from 30 to 55 °.

Pt/Nb-SnO_2 was analysed by X-ray fluorescence, in order to determine the Pt amount effectively on the support. The samples were prepared by grinding 50 mg of Pt/Nb-SnO_2 with 25 mg of cellulose. The recovered powder was then placed in a cavity in the H_3BO_3 matrix subsequently pressed, in order to obtain a pellet of 32 mm diameter with scanned surface of ca. 12 mm. The same protocol was utilized to prepare four standards using 15, 20, 25 and 30 $\%_{wt}$ of Pt black (Alfa Aesar) and Nb-SnO_2 to obtain a calibration line. The analyses were performed with a PANalytical Axios Max spectrometer fitted with a Rh (4 kW) tube, and equipped with a LiF200 crystal and Omnian software.

Ex situ electrochemical characterisation of Pt/Nb-SnO_2 loose-tubes

The *ex situ* electrochemical analyses were carried out in a conventional three-electrode cell consisting of a glassy carbon rotating disk electrode (RDE) (working electrode, geometric area of 0.196 cm^2), a reversible hydrogen electrode (reference electrode, RHE) and a platinum wire (counter electrode). A Pine bipotentiostat model AFCBP1 was used. All the potential values are referred to the RHE and the current densities are reported as current per geometric electrode area.

In order to prepare the catalyst ink, 5 mg of the Pt/Nb-SnO_2 electrocatalyst were dispersed in 10 µL milli-Q water, 0.20 mL of ethanol (Aldrich) and 10 µL 5 $\%_{wt}$ Nafion® solution in alcohols (Aldrich). For the reference, 5 mg of 50 wt. % Pt/C (Alfa Aesar) were mixed with 25 µL of milli-Q water, 0.35 mL of ethanol (Aldrich) and 25 µL of the 5 $\%_{wt}$ Nafion® solution in alcohols (Aldrich). The catalyst inks were sonicated (VWR Ultrasonic Cleaner) for 15 min. Aliquots of 3.8 µL of the Pt/C ink or 5 µL of the Pt/Nb-SnO_2 ink were then deposited onto the RDE surface with a micropipette and dried in air. The Pt loading was 121.7 µg cm^{-2} for Pt/Nb-SnO_2 and 121.2 µg cm^{-2} Pt/C.

Cyclic voltammetry was performed in N_2 saturated 0.1 M $HClO_4$. For durability experiments 2000 cycles were performed between 0.05 V and 1.2 V with a scan rate of 50 mV s^{-1}. The ECSA was evaluated before and after cycling. Its calculation was based on

hydrogen adsorption peaks in the range 0.05 V to 0.4 V vs RHE after double-layer correction, assuming a monolayer hydrogen adsorption charge of 210 µC cm^{-2} for the Pt surface.

A diluted ink was used for the investigation of the catalytic activity towards the ORR and led to Pt loadings of 14.2 µg cm^{-2} for Pt/Nb-SnO_2 and 10.5 µg cm^{-2} for Pt/C. The ORR polarisation curves were recorded using linear sweep voltammetry at 1600 rpm in O_2 saturated 0.1 M $HClO_4$. The potential was varied from 1.0 to 0.2 V vs RHE at a scan rate of 5 mV s^{-1}. The total current was first corrected for the background current measured in the N_2-saturated corresponding electrolyte and then for diffusion limiting using the Koutecky-Levich equation.

Preparation of Pt/Nb-SnO_2 based MEA and *in situ* electrochemical characterisation

GDEs for the anode were purchased from Alfa Aesar. Pt loading was 0.4 mg cm^{-2}. Nafion® 212 membranes (Ion Power) were treated before assembly with the electrodes using the following procedure. They were immersed in a 3 % v/v H_2O_2 solution (30 % wt., Carlo Erba Reagents), which was stirred for 1 h at 100 °C. After washing with water, the membranes were immersed in a 50 % w/w solution of HNO_3 (65 % wt., Sigma Aldrich) and stirred for 30 minutes at room temperature. Finally, the membranes were washed, immersed in a 1 M solution of H_2SO_4 (95 wt.%, Sigma Aldrich) for 1 h at 100 °C and rinsed again with water.

The Pt/Nb-SnO_2 and Pt/C based cathode loaded with 0.5 mg cm^{-2} of Pt was prepared with the following method. A mixture of 9.5 mg of Pt/Nb-SnO_2 or 4 mg Pt/C catalyst (Alfa Aesar), 46 µL of a 5 % wt. Nafion® solution (Sigma-Aldrich), 400 µL of water and 2 mL of ethanol was sonicated for at least 30 min and sprayed-coated on a GDL (4 cm^2, Sigracet 10 BC).

The MEA was assembled by pressing the electrodes and membrane at 140 °C for 2 min at 25 MPa. The MEA was then incorporated in the fuel cell setup using fluorinated ethylene propylene (FEP) gaskets at 10 - 15 % compression. The MEA conditioning step was performed at 0.5 A cm^{-2} overnight at 100 % RH and 80 °C. Polarization curves were recorded under H_2/O_2 (stoichiometry 1.5/2) by setting the current density and measuring the cell potential. A back-pressure of 1 bar was applied (2 bar absolute pressure).

An accelerated stress test (AST), applied in the fuel cell at 80 °C, consisted of a square-wave type voltage cycle, holding at 0.9 V for 3 sec and at 1.4 V for 3 sec, and repeating 1200 times[31]. Impedance spectroscopy measurements in the range 20 kHz to 100 mHz were performed at 0.1 A cm^{-2} to measure the resistance in the MEA before and after the voltage cycling. BSE-SEM analysis of the MEA sections was performed after the AST.

Results and discussion

Structure and morphology of Pt/Nb-SnO_2 loose-tubes

The morphology of the electrospun Nb-SnO_2 before and after loading with Pt was characterised by scanning and transmission microscopies. The micrograph in Figure 1 a clearly indicates the fibre-in-tube or "loose-tube" structure of the support with an average diameter of ca. 300 nm. As depicted in the images in Figure 1 b-c, Pt nanoparticles with an average diameter of 3 nm are homogeneously dispersed on the inner and outer surface of the tubes.

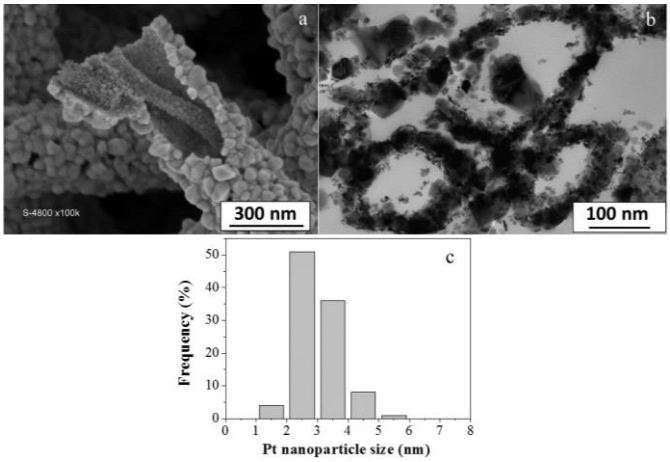

Figure 1. FE-SEM micrographs of bare Nb doped SnO_2 loose-tubes (a) and TEM micrograph of a microtomed section of a Pt catalysed support (b). Pt nanoparticle size distribution histogram (c).

From X-ray fluorescence measurements, the Pt loading on Nb-SnO_2 was determined as being 21 %$_{wt}$. The structural analysis of Pt supported on Nb-SnO_2 loose-tubes is shown in Figure 2. As already evidenced by previous XRD and Raman analyses[30], Nb-SnO_2 loose-tubes adopt the tetragonal $P4_2/mnm$ cassiterite structure (JCPDS 41-1445). The two broad peaks corresponding to Pt (111) and Pt (200) at 40.0 and 46.2 ° 2 theta, respectively, indicate the small size of the Pt particles. Indeed, the Pt crystallite size calculated from the XRD pattern in Figure 2 using the Scherrer equation is 4 nm, in good agreement with the TEM observations.

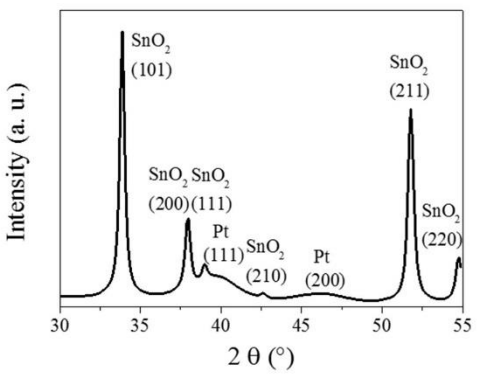

Figure 2. XRD pattern of Pt supported on Nb doped SnO_2 loose-tubes.

Ex situ electrochemical characterisation

Cyclic voltammetry (CV) measurements were performed in acidic medium on Pt/Nb-SnO_2 and for comparison on commercial Pt/C. The voltammograms in Figure 3 present the characteristic hydrogen adsorption/desorption peaks in the low potential region and Pt oxide formation and reduction in the high

potential region. The Pt electrochemical surface area (ECSA) was calculated from the hydrogen adsorption peak, and had a value of 27 m^2 g^{-1} for Pt/Nb-SnO_2. Tsukatsune *et al.*[32] reported a similar surface area of 21.4 m^2 g^{-1} for 20 % Pt/$Sn_{0.98}Nb_{0.02}O_2$. The ECSA values decreased as a consequence of cycling between 0.05 and 1.2 V vs RHE, as indicated by a decrease in the integrated area of the H adsorption peaks (Figure 3).

The surface area loss over time was stronger for the carbon-based electrode than for the tin oxide based one. Indeed, the ECSA of Pt/C decreased much faster with potential cycling than with Pt/Nb-SnO_2. After 2000 cycles, the former retained only 12 % of its electroactive area, while the latter retained 76 % (Table 1).

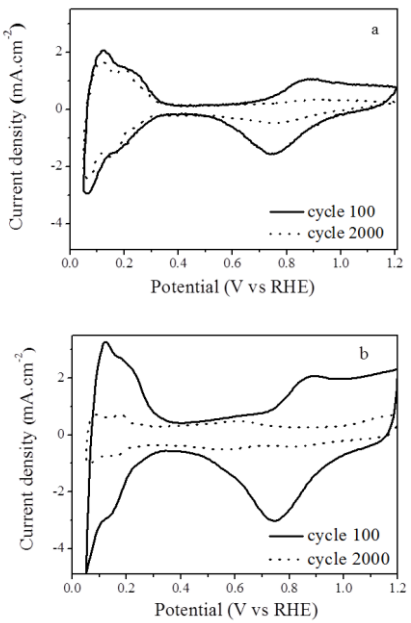

Figure 3 Cyclic voltammograms in N_2 purged 0.1 M $HClO_4$ of 21 % Pt/$NbSnO_2$ (a) and 50 % Pt/C (b) before and after voltage cycling.

Table 1. ECSA loss upon cycling for Pt/Nb-SnO_2 and Pt/C.

ECSA, m^2 g^{-1}	21 % Pt/Nb-SnO_2	50 % Pt/C
Cycle 20	27	33
Cycle 2000	21	4

These results can be explained in terms of the corrosion of the carbon support during the prolonged potential cycling. The Pt particles underwent growth, dissolution, migration/agglomeration or detachment from the corroded support, leading to the loss of electroactive area[33,34]. On the other hand, Pt supported on the oxide loose-tubes showed a significantly higher stability to cycling to high voltage. This result is attributed to the corrosion resistance of the support[30] as well as to strong Pt-SnO_2 interactions, evidence for which has been provided in recent reports on tin oxide based PEMFC cathodes[9,31].

Furthermore, the anodic current due to the formation of platinum oxides and the cathodic current due to their reduction were observed to decrease, consistent with studies[35] that have attributed this behaviour to the interaction between Pt and SnO_2, which becomes stronger as the Pt particle density decreased. The activity of Pt/Nb-SnO_2 towards oxygen reduction was also evaluated and compared to that obtained with conventional Pt/C. For both electrodes the onset potential of the polarisation curves was around 0.96 V. The ORR mass activities at 0.9 V were 34 and 87 A g^{-1}_{Pt} for 21 % Pt/Nb-SnO_2 and 50 % Pt/C, respectively. The value concerning the oxide supported Pt is in agreement with recent results obtained with Pt deposited onto Sb doped SnO_2 (*e.g.* 15.5 A g^{-1}_{Pt} at 0.9 V[16] and 94 A g^{-1}_{Pt} at 0.85 V[20]).

Tafel slopes have been calculated in the kinetically controlled range (Figure 4). For the Pt/C electrocatalyst the slope of -68 mV dec^{-1} is typical of platinum at low overpotentials[36,37]. A different slope of -103 mV dec^{-1} has been obtained for Pt/Nb-SnO_2, as already reported for Pt nanoparticles supported on SnO_2[8]. It is known that on polycrystalline Pt in acidic media in low current density range, a theoretical Tafel slope of -60 mV dec^{-1} is obtained, corresponding to the ORR proceeding on oxide-covered Pt, while at high current densities, Tafel slope rises to -120 mV dec^{-1}, indicating a reaction occurring at an oxide-free surface with a transfer coefficient α of 0.5[38]. The high value obtained with the tin oxide support, typical of the reduced metal surface, could arise from the capability of SnO_2 of adsorbing oxygen species[39], thus partially reducing the Pt surface even at high potentials.

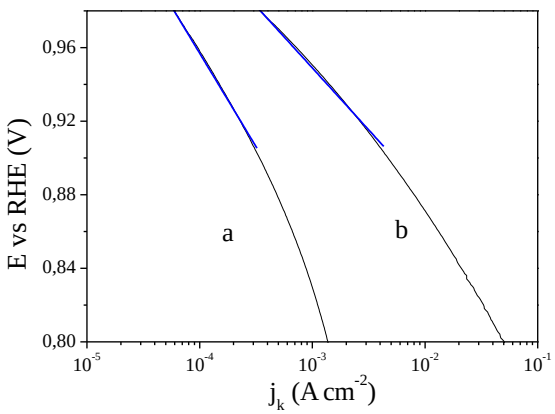

Figure 4. Tafel plots for the oxygen reduction reaction at 21 % Pt/Nb-SnO_2 (a) and 50 % Pt/C (b). In blue, linear extrapolation for Tafel slope determination.

In situ electrochemical characterisation

Figure 5 shows the current density - voltage curves of the two MEAs with the Pt/Nb-SnO_2 catalyst and with the commercial Pt/C catalysts recorded on H_2/O_2 before and after *in situ* voltage cycling to 1.4 V (1200 cycles). The initial open circuit voltage (OCV), 0.960 V for the MEA with the Pt/Nb-SnO_2 cathode, and 0.962 V for the reference MEA (Pt/C cathode), is practically unchanged after the accelerated stress test. The IV curves of Figure 5 show that the MEA with the Pt/Nb-SnO_2 electrode

provides lower current density at a given cell voltage (Figure 5 a) than the reference MEA with a Pt/C cathode (Figure 5 b), the former displaying a maximum power density of 0.41 W.cm^{-2} at a current density of 1 A cm^{-2} compared to 0.96 W.cm^{-2} for Pt/C. This result is probably a consequence of the relatively lower electron conductivity of the oxide compared to the carbon support[40]. The high initial voltage drop at low current density for the Pt/NbSnO$_2$ based MEA may be assigned to lower ORR activity compared to that of Pt/C electrocatalyst[8,41] as described above for the *ex situ* analysis.

One of the most important observations of this work concerns the stability of the non-carbon cathode to voltage cycling, when the performance of Pt/Nb-SnO$_2$-based MEA was observed to slightly increase from 0.41 to 0.47 W cm^{-2} at 1 A cm^{-2} after 600 cycles (Figure 5)[41] while, in contrast, for the Pt/C-based MEA a dramatic drop in performance was observed.

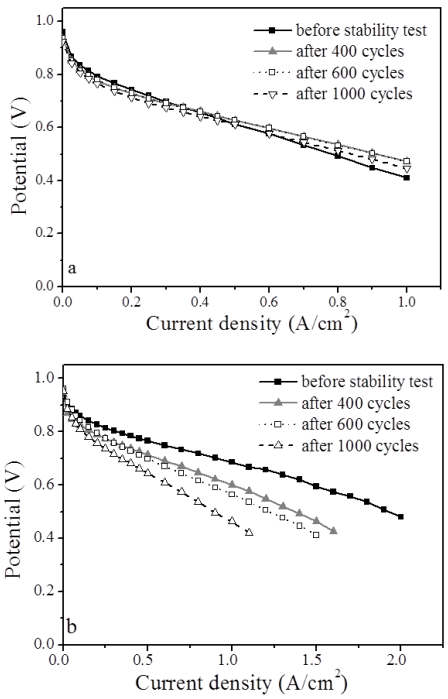

Figure 5. I-V characteristics of MEA with Pt/Nb-SnO$_2$ (a) and Pt/C (b) before and after *in situ* voltage cycling.

There was a significant change in both the ohmic and the mass transfer regions, whereas the initial potential drop remains relatively unchanged. This indicates that the loss of performance for the reference MEA (Pt/C cathode) is likely due to deterioration in the conductivity of the catalyst supports and in the mass-transport behaviour of the cathode. Carbon corrosion leads to functionalization of the carbon surface[42], which results in an increase in the hydrophilicity of the catalyst layer and high mass-transport overpotentials. The fuel cell performance loss is also related to a thinning of the catalyst layer due to detachment and migration of Pt nanoparticles as a result of carbon corrosion as well as Pt dissolution and migration (see SEM observations after AST). The higher stability of the tin oxide based electrocatalyst at high potentials is explained by their greater corrosion resistance, already demonstrated *ex situ*[30], which allows retention of morphology and conductivity.

SEM observations after AST

The morphology of the MEAs after 1200 voltage cycles to 1.4 V was investigated using electron microscopy. Figure 6 shows a typical BSE-FESEM micrograph of the cross-section of Pt/Nb-SnO$_2$ and Pt/C electrocatalyst layers. In Figure 6 a and c Pt-decorated Nb-SnO$_2$ tubes are observed with no collapse of the loose-tube structure after either the MEA fabrication that had comprised sonication and spraying of the catalyst ink, and hot-pressing, or following voltage cycling. In contrast, the Pt/C electrodes of Figure 6 b and d show that the nanocatalysts have undergone significant aggregation. Furthermore, thinning of the catalyst layer can be observed due to the detachment and migration of the Pt nanoparticles.

To provide further evidence for the higher stability of the tin oxide based electrode, FE-SEM was performed on the whole MEA cross-section. This allowed observation of the membrane and the eventual formation of a "Pt band" as reported in previous studies of degradation of PEMFC at high cathode potentials[43]. In Figure 7 bright features due to platinum may be observed, that are present not only in the electrodes but also as a band at the mid-point of the MEA. This Pt band is particularly evident in the Pt/C based MEA (Figure 7b), which is caused by platinum dissolution from the cathode, migration through the membrane and precipitation as nanoparticles, forming a bright front at the point at where hydrogen and oxygen gas pressures are equilibrated. In the case of Pt/Nb-SnO$_2$, this effect is much reduced, being mitigated (Figure 7 a) by the higher corrosion resistance of the support as well as to the strong interaction between Pt and SnO$_2$[44].

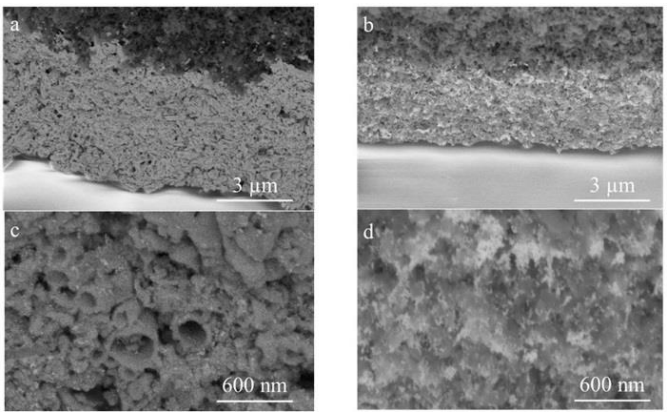

Figure 6. SEM micrographs (BSE mode) of cathodes with Pt/NbSnO$_2$ (a, c) and Pt/C (b, d) after 1200 cycles 0.9-1.4 V.

Impedance spectroscopy

In order to evaluate the charge transport properties of the Nb-doped SnO$_2$ loose-tubes in comparison with the carbon based electrocatalyst in fuel cell electrodes, Nyquist plots were

obtained by electrochemical impedance spectroscopy before and after the stability test.

A single impedance arc is observed in the Nyquist plot of Figure 8, the diameter of which corresponds to the charge transfer (R_{ct}) of the oxygen reduction reaction due to the fast hydrogen oxidation reaction kinetics. A Randles model is usually used to describe a single semicircle loop, where double-layer capacitance is replaced by a constant phase element (CPE) due to porous structure of the electrode[45]. The R_{ct} for the SnO_2 based electrode was greater than that for carbon-based cathode, as shown in Table 2. This result corroborates the lower initial fuel cell performance observed earlier. However, the R_{ct} of tin oxide based MEA remains almost unchanged after voltage cycling. In contrast, R_{ct} of carbon based electrode increased dramatically from 0.503 to 0.900 Ω cm^2, clearly identifying the performance loss as arising from degradation effects at the cathode (Figures 6 and 7). The ohmic resistance obtained from the intersection of the semicircle loop with the *x* axis was higher for the MEA with the Pt/Nb-SnO_2 cathode than that for the reference MEA (Pt/C cathode), as shown in Table 2, due the lower conductivity of the ceramic support.

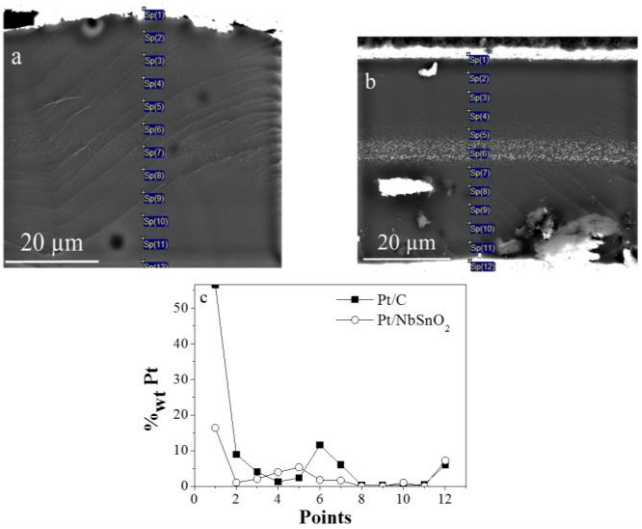

Figure 7. BSE-SEM micrographs of MEAs with Pt/Nb-SnO_2 (a) and Pt/C (b) after 1200 cycles ADT and graphic of the Pt amount as a function of the position (c).

Table 2. Ohmic and charge transfer resistance before and after AST at 0.1 A cm^{-2} for Pt/Nb-SnO_2 and Pt/C cathode based MEAs.

Number of cycles	R_{ohm}, Ω cm^2 Ohmic resistance	R_{ct}, Ω cm^2 Charge-transfer resistance
Pt/C		
0	0.071	0.503
1200	0.070	0.900
Pt/NbSnO$_2$		
0	0.095	0.835
1200	0.098	0.810

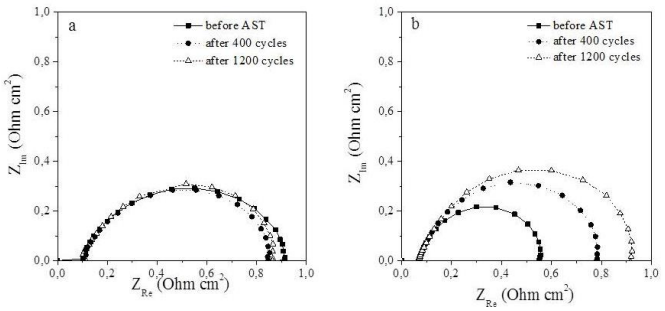

Figure 8. Nyquist plots of Pt/Nb-SnO_2 (a) and Pt/C (b) before and after voltage cycling test.

Conclusions

Nb-doped SnO_2 loose-tubes loaded with Pt nanoparticles demonstrated higher electrochemical stability than conventional Pt/C electrodes under prolonged potential cycling with good performance in the oxygen reduction reaction. Fuel cell tests confirmed the enhanced durability over time of the cathodes prepared with the alternative supports. Electron microscopy analyses performed after the in situ accelerated stress tests confirmed that the 1 D morphology was retained. Furthermore, due to the strong metal support interaction, the Pt nanoparticles did not agglomerate or detach from Nb-SnO_2, whereas in the carbon based cathode Pt was lost from the support and formed a band in the membrane. These results show the clear promise of associating doped tin oxide compositions with electrospinning to tune the support morphology and surface area and with microwave assisted polyol method to rapidly prepare monodisperse electrocatalyst particles, for preparation of cathode catalyst support for PEMFC with designed architecture and tuned corrosion resistance. This work has further highlighted the need for higher support conductivity which will require further modulation of the support composition, and increased electrocatalyst mass activity for which support architecture and porosity are key determining factors.

Acknowledgements

The research leading to these results has received funding from the Future Emerging Technologies (FET) Programme under the European Community Seventh Framework Programme (FP/2007-2013) under Grant Agreement 256821. The authors gratefully acknowledge this financial support. I.S. acknowledges the financial support from French National Research Agency (ANR-12-PRGE-0007).

Furthermore the research leading to these results has received funding from the European Research Council under the European Union's Seventh Framework Programme (FP/2007-2013) / ERC Grant Agreement n. 306682.

Notes and references

[a] Institut Charles Gerhardt, UMR CNRS 5253, Agrégats Interfaces Matériaux pour l'Energie, Université de Montpellier - 34095 Montpellier Cedex 5, France

*E-mail: sara.cavaliere@univ-montp2.fr; Fax: +33 (0)4 67 14 33 04; Tel: +33 (0)4 67 14 90 98

1. M. Wesselmark, B. Wickman, C. Lagergren and G. Lindbergh, *Electrochim. Acta*, 2010, **55**, 7590–7596.

2. A. Bauer, L. Chevallier, R. Hui, S. Cavaliere, J. Zhang, D. Jones and J. Rozière, *Electrochim. Acta*, 2012, **77**, 1–7.

3. L. Chevallier, A. Bauer, S. Cavaliere, R. Hui, J. Rozière and D. J. Jones, *ACS Appl. Mater. Interfaces*, 2012, **4**, 1752–1759.

4. S. Cavaliere, S. Subianto, L. Chevallier, D. J. Jones and J. Rozière, *Chem. Commun. (Camb).*, 2011, **47**, 6834–6836.

5. H. Chhina, S. Campbell and O. Kesler, *J. Electrochem. Soc.*, 2007, **154**, B533.

6. P. J. Kulesza, K. Miecznikowski, B. Baranowska, M. Skunik, a. Kolary-Zurowska, a. Lewera, K. Karnicka, M. Chojak, I. Rutkowska, S. Fiechter, P. Bogdanoff, I. Dorbandt, G. Zehl, R. Hiesgen, E. Dirk, K. S. Nagabhushana and H. Boennemann, *J. Appl. Electrochem.*, 2007, **37**, 1439–1446.

7. M. S. Saha, M. N. Banis, Y. Zhang, R. Li, X. Sun, M. Cai and F. T. Wagner, *J. Power Sources*, 2009, **192**, 330–335.

8. P. Zhang, S.-Y. Huang and B. N. Popov, *J. Electrochem. Soc.*, 2010, **157**, B1163.

9. F. Takasaki, S. Matsuie, Y. Takabatake, Z. Noda, a. Hayashi, Y. Shiratori, K. Ito and K. Sasaki, *J. Electrochem. Soc.*, 2011, **158**, B1270.

10. A. Ignaszak, C. Teo, S. Ye and G. Elod, *J. Phys. Chem. C*, 2010, **114**, 16488–16504.

11. M. Sudan Saha, R. Li, M. Cai and X. Sun, *Electrochem. Solid-State Lett.*, 2007, **10**, B130.

12. V. Tripković, I. Cerri, T. Nagami, T. Bligaard and J. Rossmeisl, *Phys. Chem. Chem. Phys.*, 2013, **15**, 3279–85.

13. Y. Shao, J. Liu, Y. Wang and Y. Lin, *J. Mater. Chem.*, 2009, **19**, 46–59.

14. M. Fehse, S. Cavaliere, P. E. Lippens, I. Savych, a. Iadecola, L. Monconduit, D. J. Jones, J. Rozière, F. Fischer, C. Tessier and L. Stievano, *J. Phys. Chem. C*, 2013, **117**, 13827–13835.

15. Y. Wang, T. Brezesinski, M. Antonietti and B. Smarsly, *ACS Nano*, 2009, **3**, 1373–1378.

16. E. Fabbri, a Rabis, R. Kötz and T. J. Schmidt, *Phys. Chem. Chem. Phys.*, 2014, **16**, 13672–81.

17. M. Yin, J. Xu, Q. Li, J. O. Jensen, Y. Huang, L. N. Cleemann, N. J. Bjerrum and W. Xing, *Appl. Catal. B Environ.*, 2014, **144**, 112–120.

18. Y. Senoo, K. Taniguchi, K. Kakinuma, M. Uchida, H. Uchida, S. Deki and M. Watanabe, *Electrochem. commun.*, 2015, **51**, 37–40.

19. D. J. You, K. Kwon, C. Pak and H. Chang, *Catal. Today*, 2009, **146**, 15–19.

20. N. R. Elezovic, B. M. Babic, V. R. Radmilovic and N. V. Krstajic, *J. Electrochem. Soc.*, 2013, **160**, F1151–F1158.

21. M. S. Saha, V. Neburchilov, D. Ghosh and J. Zhang, *Wiley Interdiscip. Rev. Energy Environ.*, 2013, **2**, 31–51.

22. S. Cavaliere, S. Subianto, I. Savych, D. J. Jones and J. Rozière, *Energy Environ. Sci.*, 2011, **4**, 4761–4785.

23. A. Bauer, K. Lee, C. Song, Y. Xie, J. Zhang and R. Hui, *J. Power Sources*, 2010, **195**, 3105–3110.

24. Q. Long, M. Cai, J. Li, H. Rong and L. Jiang, *J. Nanoparticle Res.*, 2010, **13**, 1655–1662.

25. L. Yang, M. Vukmirovic, D. Su, K. Sasaki, J. Herron, M. Mavrikakis, S. Liao and R. R. Adzic, *J. Phys. Chem. C*, 2013, **117**, 1748–1753.

26. K. Senevirathne, R. Hui, S. Campbell, S. Ye and J. Zhang, *Electrochim. Acta*, 2012, **59**, 538–547.

27. I. Savych, J. Bernard d'Arbigny, S. Subianto, S. Cavaliere, D. J. Jones and J. Rozière, *J. Power Sources*, 2014, **257**, 147–155.

28. A. B. Suryamas, G. M. Anilkumar, S. Sago, T. Ogi and K. Okuyama, *Catal. Commun.*, 2013, **33**, 11–14.

29. S. Sago, A. B. Suryamas, G. M. Anilkumar, T. Ogi and K. Okuyama, *Mater. Lett.*, 2013, **105**, 202–205.

30. S. Cavaliere, S. Subianto, I. Savych, M. Tillard, D. J. Jones, J. Rozière and D. J. Jones, *J. Phys. Chem. C*, 2013, **117**, 18298–18307.

31. K. Kakinuma, Y. Chino, Y. Senoo, M. Uchida, T. Kamino, H. Uchida, S. Deki and M. Watanabe, *Electrochim. Acta*, 2013, **110**, 316–324.

32. T. Tsukatsune, Y. Takabatake and Z. Noda, *ECS Trans.*, 2013, **58**, 1251–1257.

33. Y. Shao, G. Yin and Y. Gao, *J. Power Sources*, 2007, **171**, 558–566.

34. Y. Sugawara, A. P. Yadav, A. Nishikata and T. Tsuru, *J. Electroanal. Chem.*, 2011, **662**, 379–383.

35. M. Nakada, A. Ishihara, S. Mitsushima, N. Kamiya and K. Ota, *Electrochem. Solid-State Lett.*, 2007, **10**, F1.

36. C. Song and J. Zhang, in *PEM Fuel Cell Electrocatalyst and Catalyst Layers. Fundamentals and Applications*, ed. J. Zhang, Springer-Verlag, 2008, pp. 89–134.

37. N. Wakabayashi, M. Takeichi, M. Itagaki, H. Uchida and M. Watanabe, *J. Electroanal. Chem.*, 2005, **574**, 339–346.

38. D. A. Walsh, A. Ejigu, J. Smith and P. Licence, *Phys. Chem. Chem. Phys.*, 2013, **15**, 7548–54.

39. S. Mukerjee and J. McBreen, *J. Electrochem. Soc.*, 1999, **146**, 600–606.

40. K. Kanda, Z. Noda, Y. Nagamatsu, T. Higashi, S. Taniguchi, S. M. Lyth, a. Hayashi and K. Sasaki, *ECS Electrochem. Lett.*, 2014, **3**, F15–F18.

41. T. Higashi, *ECS Trans.*, 2013, **58**, 1293–1299.

42. Y. Yang and Z. G. Lin, *J. Appl. Electrochem.*, 1995, **25**, 259–266.

43. J. Peron, Y. Nedellec, D. Jones and J. Rozière, *J. Power Sources*, 2008, **185**, 1209–1217.

44. S. J. Tauster, *Acc. Chem. Res.*, 1987, **20**, 389–394.

45. X. Yuan, H. Wang, J. Colinsun and J. Zhang, *Int. J. Hydrogen Energy*, 2007, **32**, 4365–4380.

